

## Supporting Information

### Halogen Bonds Regulating Structures and Optical Properties of Hybrid Iodobismuthate Perovskites

General information.....	2
Synthesis of the hybrids.....	2
Crystallographic analysis.....	2
Powder X-ray diffraction patterns.....	4
Hirshfeld surface analysis.....	5
Stability in water and in air.....	8
Structural transformation.....	9
Thermochromics.....	9
Other characterizations.....	11
Theoretical computations.....	15
References.....	30

## General information

All the solvents used for crystal growth are reagent grade. All the chemicals and the solvents were used as received without further treatment. iodo substituted N-methyl pyridinium (IPyMe·I) was easily prepared by the reaction of 4-iodopyridine and methyl iodide. [1]

## Synthesis of the hybrids

**Synthesis of C\_1:** IPyMe·I (0.04 mmol, 13.9 mg) and BiI<sub>3</sub> (0.04 mmol, 23.6 mg) were respectively dissolved in 8 ml and 4 ml methanol. Immediately at mixing the two solutions, orange amorphous precipitate (**P\_1**) was produced in the system. Keeping the mixture undisturbed for 2 hours, needle crimson crystals **C\_1** and granular orange red crystals **C\_2** appear in the system. The granular crystals (**C\_2**) further transform to needle crystals (**C\_1**) when kept in the pristine solution for 1 day.

### Synthesis of C\_2:

*Method 1.* IPyMe·I (0.06 mmol, 20.8 mg) and BiI<sub>3</sub> (0.04 mmol, 23.6 mg) were first separately dissolved in 8 ml and 4 ml methanol. Immediately at mixing the two solutions, orange amorphous precipitate (**P\_1**) was produced in the system. Keeping the mixture undisturbed for 2 hours, needle crimson crystals **C\_1** and granular orange red crystals **C\_2** appear in the system. The needles (**C\_1**) further transform to **C\_2** when kept in the pristine solution for 2 days.

*Method 2.* BiI<sub>3</sub> (0.02 mmol, 11.8 mg) and IMePy·I (0.06 mmol, 20.8 mg) were weighed and added to a sealed tube. The contents were dissolved in 1 ml 47% aqueous HI via ultrasonication for 1 minute, followed by heating at 100 °C in oven for 3 hours. Upon slow cooling to room temperature, pure orange prismatic crystals (**C\_2**) were obtained. Store it in acetonitrile solution.

### Synthesis of C\_3:

*Method 1.* BiI<sub>3</sub> (0.02 mmol, 11.8 mg) and IMePy·I (0.06 mmol, 20.8 mg) were weighed and added to a sealed tube. The contents were dissolved in 1 ml 57% aqueous HI and then 221.8 mg sodium hypophosphite was added. The mixture was heated at 100 °C for 3 hours in an oven. Upon slow cooling to room temperature, pure orange block crystals (**C\_3**) were obtained.

*Method 2.* BiI<sub>3</sub> (0.02 mmol, 11.8 mg) and IMePy·I (0.06 mmol, 20.8 mg) were weighed and added to a sealed tube. The contents were dissolved in 1 ml 47% aqueous HI via ultrasonication for 1 minute, followed by heating at 100 °C in oven for 3 hours. Upon slow cooling to room temperature, **C\_2** were obtained. **C\_2** in solution for around 3 days would fully transform to **C\_3**.

## Crystallographic analysis

The crystallographic data were collected at 296 K with a Bruker APEX-II CCD diffractometer using Mo-Kα ( $\lambda = 0.71073 \text{ \AA}$ ) radiation. The data at other temperature were collected on a Bruker D8 VENTURE with METALJET Ga-Kα ( $\lambda = 1.34139 \text{ \AA}$ ) radiation and PHOTON II detector. APEX-III software suite [2] was used for both data collection and processing. The intensities were corrected for absorption using the Multi-

scan, where SADABS model [3] was used. Both structures were solved by the intrinsic phasing algorithm within SHELXT [4] and refined by full-matrix least-squares methods using OLEX2 [5], which utilizes the SHELXL-2015 module [6]. All atoms in the structures were refined with anisotropic thermal parameters.

**Table S1.** Crystallographic data and structural refinements at different temperatures.

Complex	C_1	C_2	C_3
<b>Formula</b>	BiI <sub>4</sub> ·C <sub>6</sub> H <sub>7</sub> IN	Bi <sub>2</sub> I <sub>9</sub> ·3(C <sub>6</sub> H <sub>7</sub> IN)	BiI <sub>6</sub> ·3(C <sub>6</sub> H <sub>7</sub> IN)
<b>M<sub>r</sub></b>	1889.23	2220.14	1630.46
<b>T / K</b>	296	296	296
<b>Crystal system</b>	Triclinic	Triclinic	Monoclinic
<b>Space group</b>	<i>P</i> -1	<i>P</i> -1	<i>P</i> 2 <sub>1</sub> /n
<b>a/Å</b>	7.7329 (16)	10.6214 (19)	10.409 (2)
<b>b/Å</b>	10.364 (2)	12.362 (2)	13.542 (3)
<b>c/Å</b>	11.706 (2)	16.562 (3)	12.252 (2)
<b>α/°</b>	70.549 (3)	79.662 (3)	90
<b>β/°</b>	81.104 (3)	84.417 (3)	95.906 (3)
<b>γ/°</b>	88.664 (3)	89.782 (3)	90
<b>V/Å<sup>3</sup></b>	873.6 (3)	2129.0 (7)	1717.9 (6)
<b>Z</b>	1	2	2
<b>μ (mm<sup>-1</sup>)</b>	18.90	16.97	13.23
<b>Crystal size (mm)</b>	0.08×0.08×0.18	0.1×0.11×0.27	0.1×0.12×0.12
<b>No. of measured, independent and observed [<i>I</i> &gt; 2s(<i>I</i>)] reflections</b>	9836, 5648, 4266	23307, 13292, 6792	13160, 3528, 3214
<b>R<sub>int</sub></b>	0.027	0.037	0.044
<b>(sin θ/λ)<sub>max</sub> (Å<sup>-1</sup>)</b>	0.753	0.739	0.627
<b>R[F<sup>2</sup> &gt; 2s(F<sup>2</sup>)]</b>	0.038	0.044	0.027
<b>wR(F<sup>2</sup>)</b>	0.106	0.100	0.065
<b>S</b>	1.00	0.96	1.13
<b>Δρ<sub>max</sub>, Δρ<sub>min</sub> (e Å<sup>-3</sup>)</b>	1.85, -1.42	2.20, -1.75	0.78, -0.86
<b>CCDC Number</b>	2234400	2234401	2234399

<sup>a</sup> R<sub>1</sub> =  $\sum ||F_o| - |F_c|| / \sum |F_o|$ . wR<sub>2</sub> =  $[\sum w(F_o^2 - F_c^2)^2 / \sum w(F_o^2)^2]^{1/2}$ .

- Powder X-ray diffraction patterns

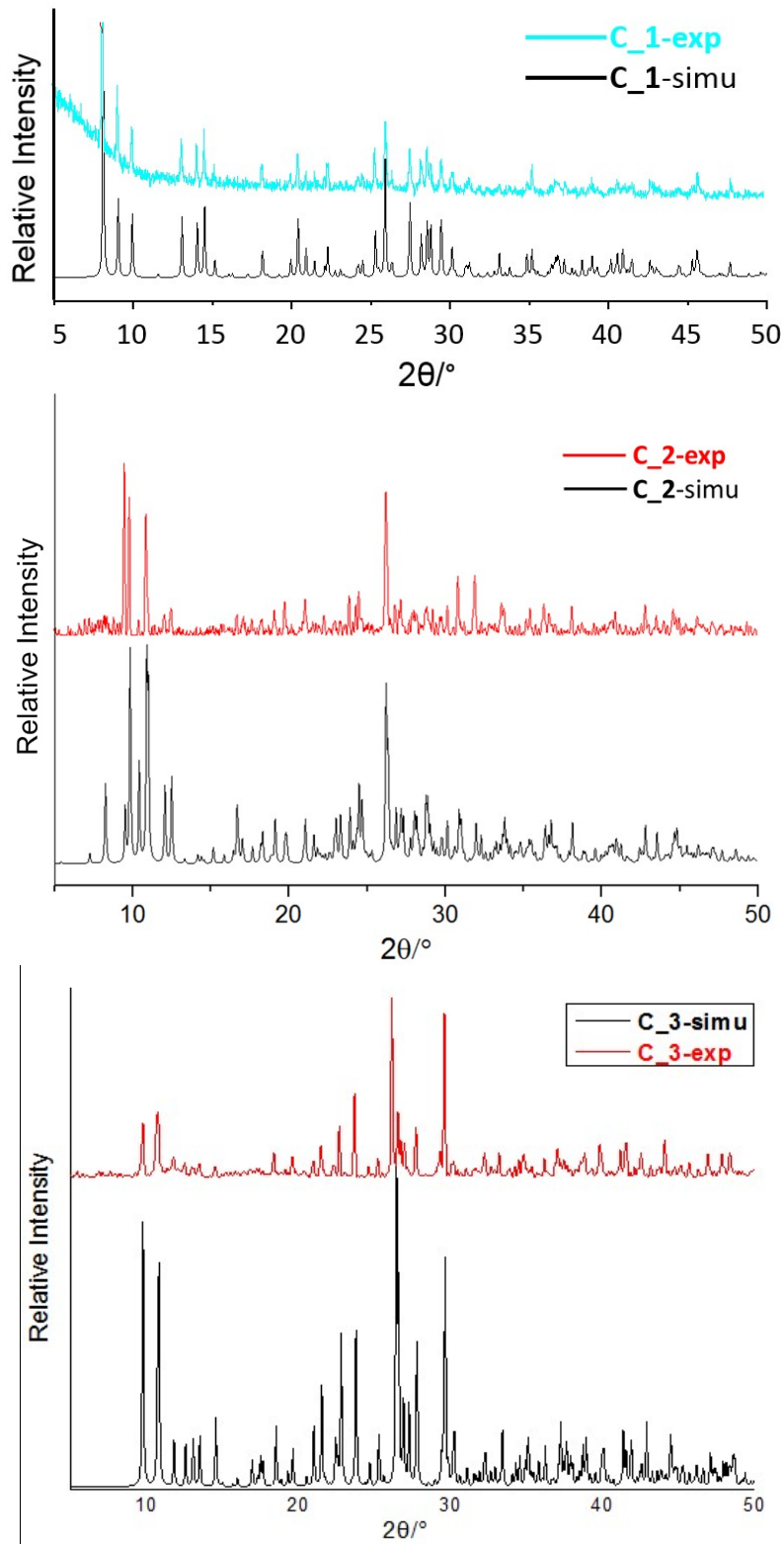


Figure S1. Powder X-ray diffraction patterns for **C\_1**, **C\_2** and **C\_3**.

- **Hirshfeld surface analysis**

Hirshfeld surface analysis was calculated at B3LYP/6-31G(d,p) level with Tonto [7], which was implemented in CrystalExplorer [8].

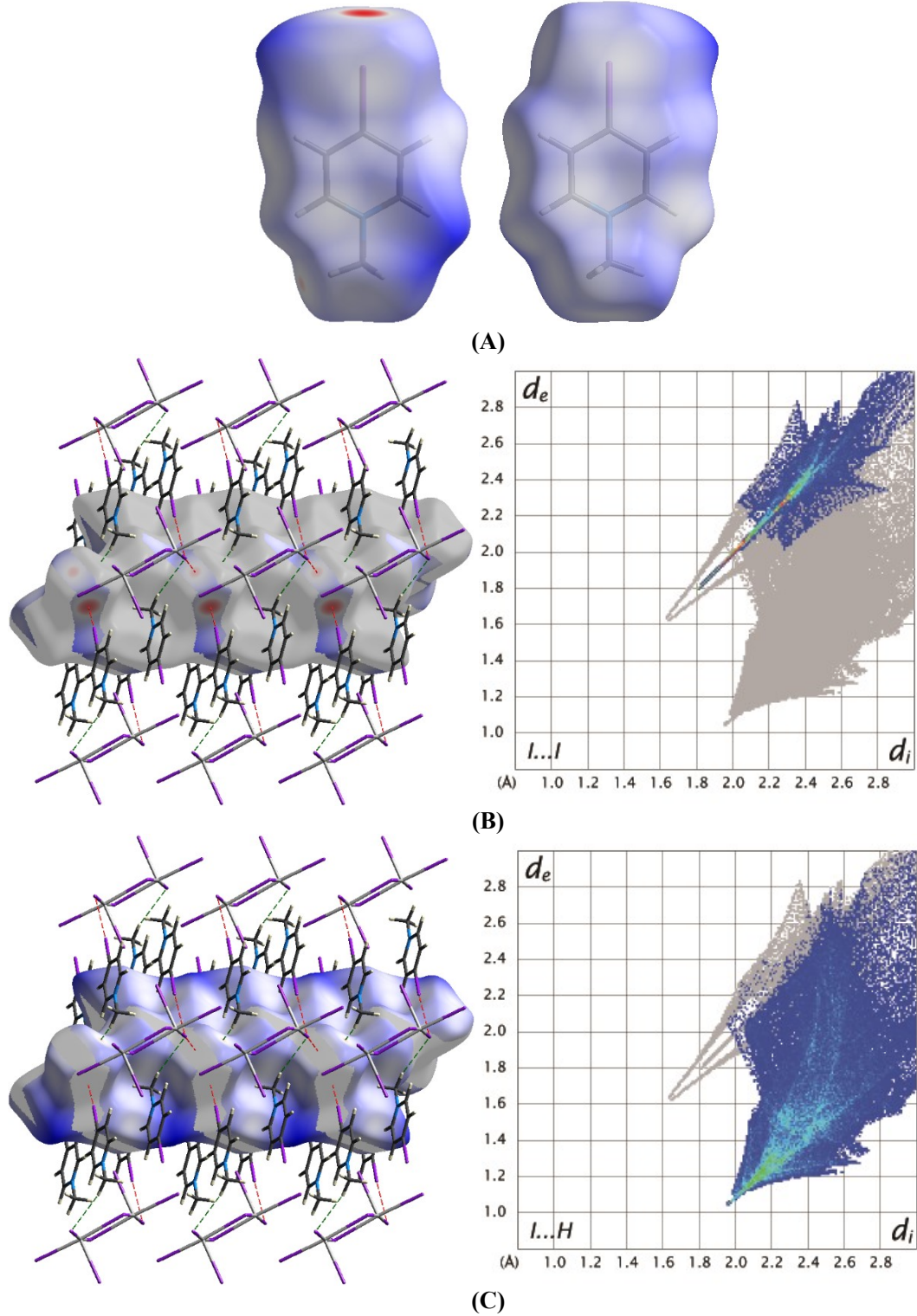


Figure S2. The Hirshfeld surface (A), and finger print plots showing the interspecies interactions (B and C for  $I \cdots I$  and  $I \cdots H$ , respectively) in **C-1**. The  $I \cdots I$  interactions take up to 20.3% and  $I \cdots H$  interactions take up to 74.5% of the surface contacts.

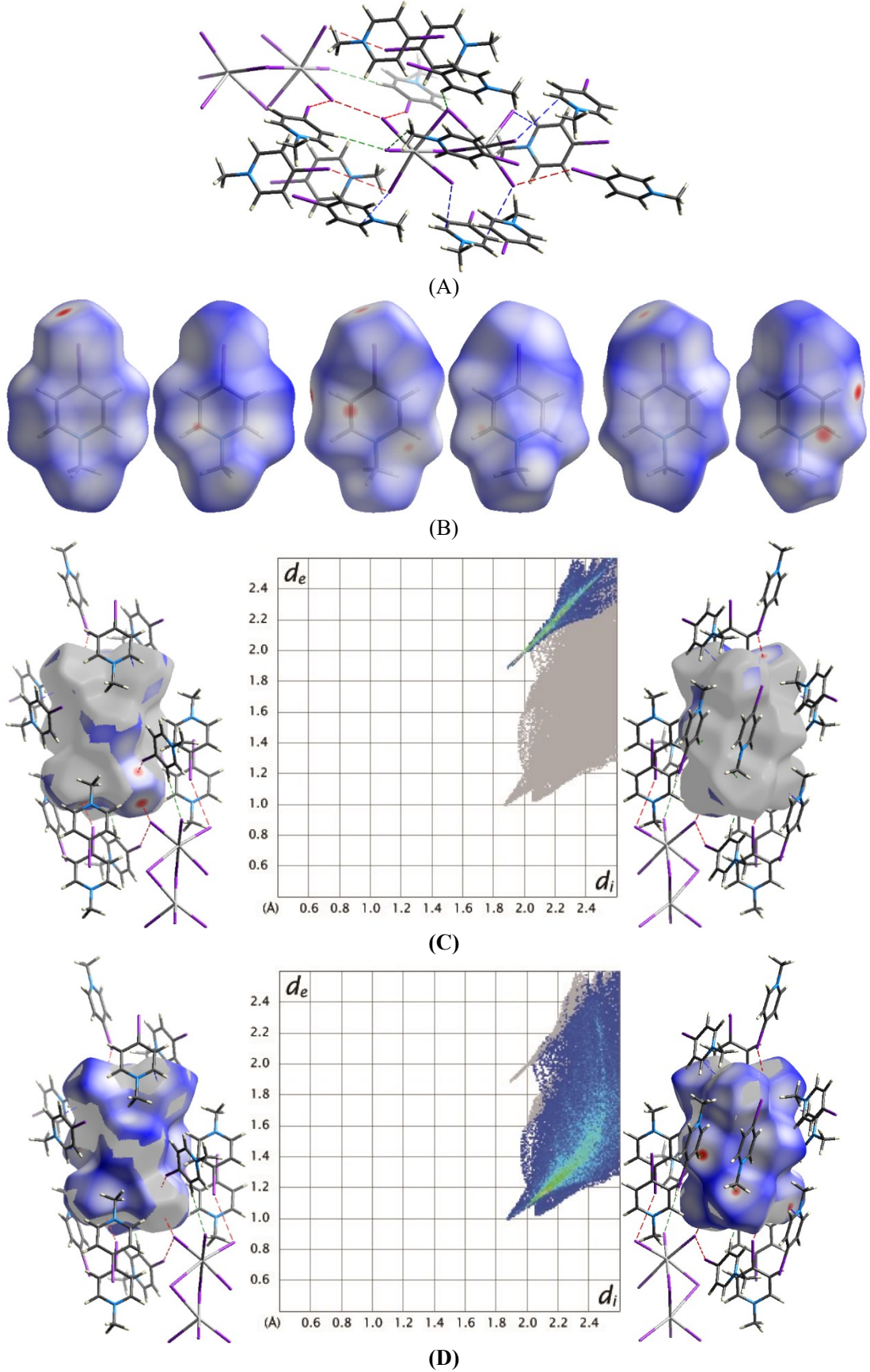


Figure S3. The interacting species (A), Hirshfeld surface of the independent organic cations (B), and finger print plots showing the interspecies interactions (C and D for  $\text{I}\cdots\text{I}$  and  $\text{I}\cdots\text{H}$ , respectively) in **C\_2**. The  $\text{I}\cdots\text{I}$  interactions take up to 16.0% and  $\text{I}\cdots\text{H}$  interactions take up to 74.3% of the surface contacts.

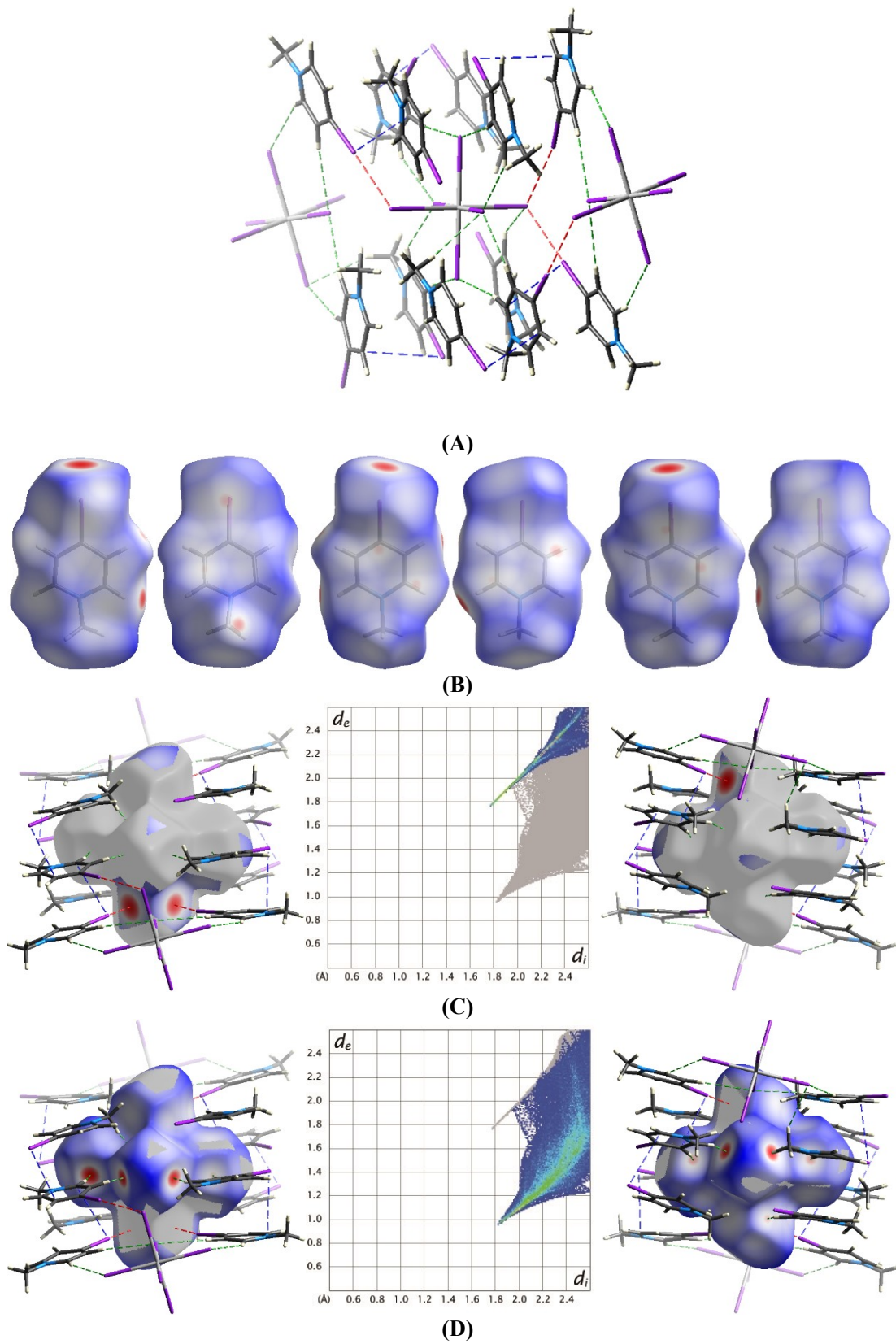


Figure S4. The interacting species (A), Hirshfeld surface of the independent organic cations (B), and finger print plots showing the interspecies interactions (C and D for I···I and I···H, respectively) in C\_3. The I···I interactions take up to 14.8% and I···H interactions take up to 84.4% of the surface contacts.

- Stability in water and in air

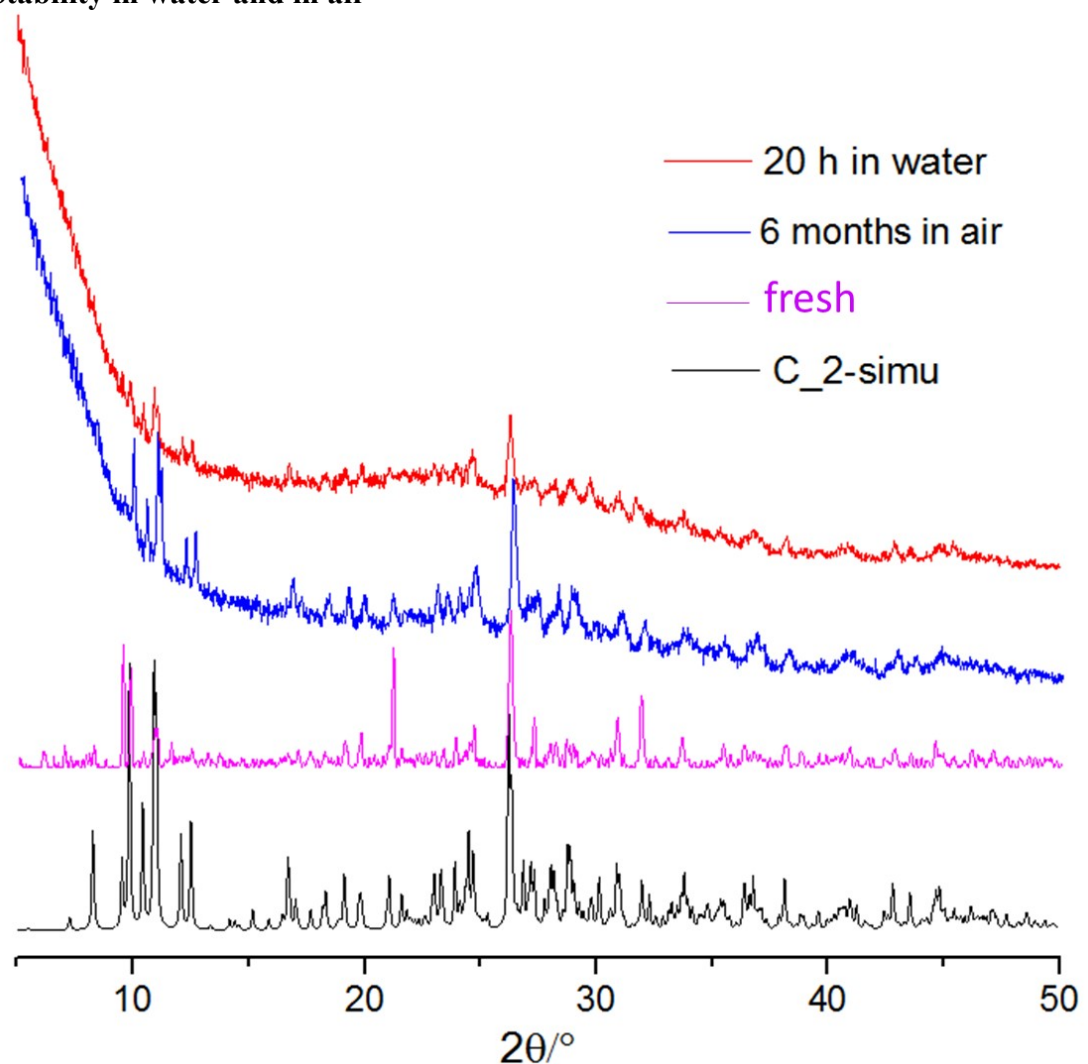


Figure S5. The PXRD patterns for C\_2 freshly synthesized, after 6 months in air and treated by water for 20 hours.

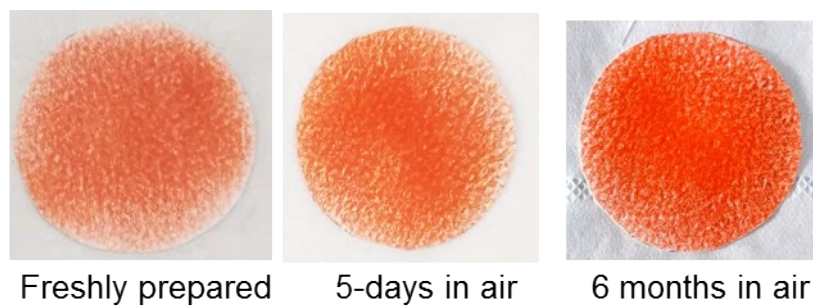


Figure S6. Photographs of the crystalline powder of C\_2 in air.

- Structural transformation

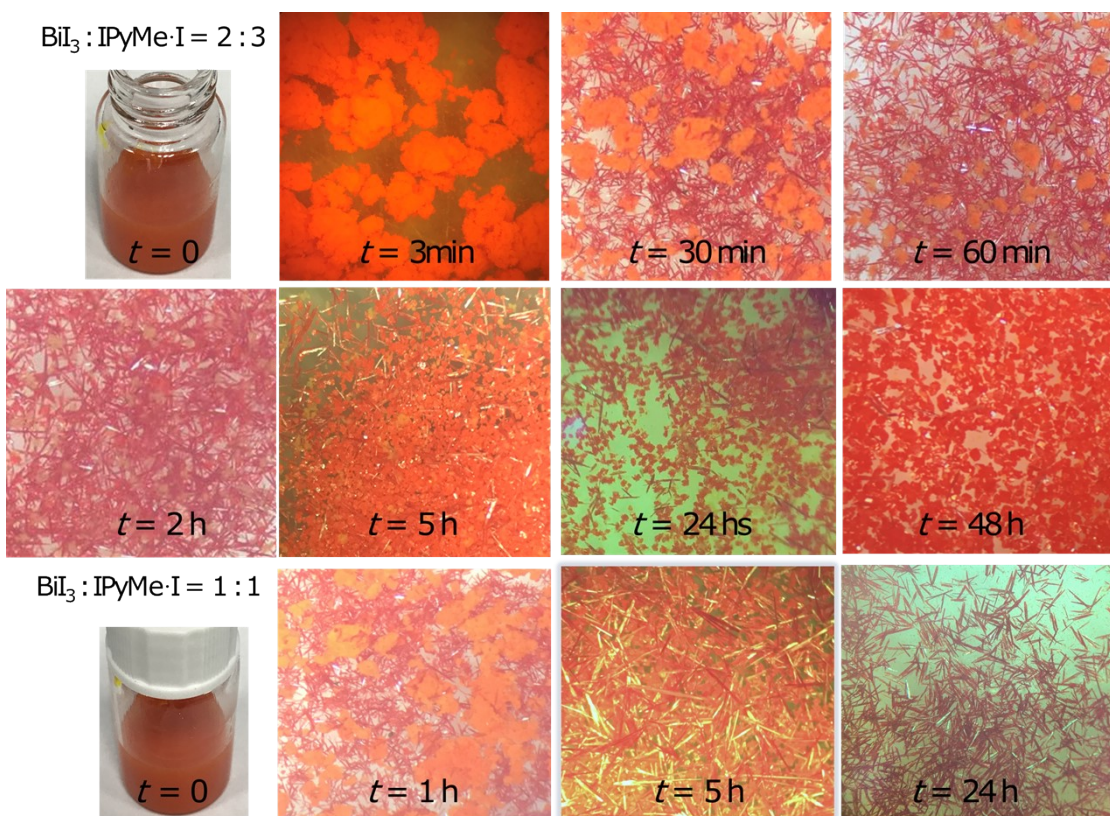


Figure S7. The structural transformation with different initial  $\text{BiI}_3$  and  $\text{IPyMe-I}$  ratio in MeOH solution.

- Thermochromics

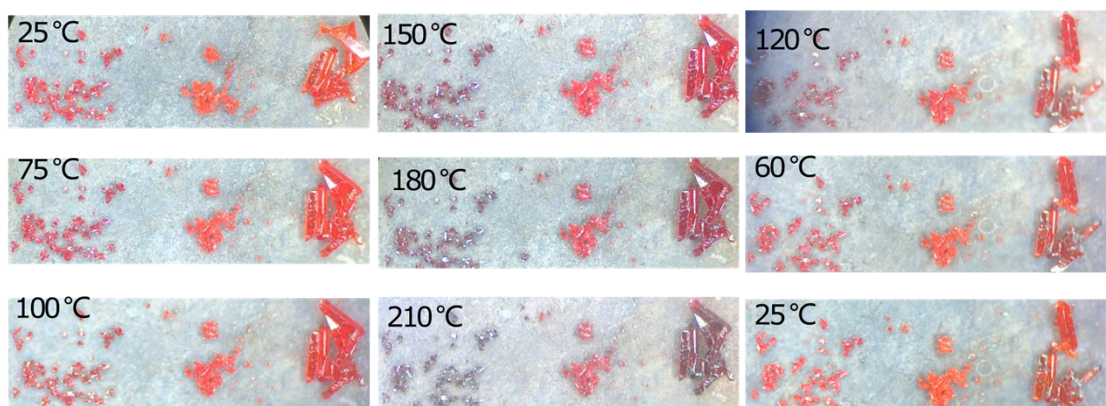


Figure S8. The photographs for the crystals of **C\_1** (left), **C\_2** (middle) and **C\_3** (right) at different temperatures.

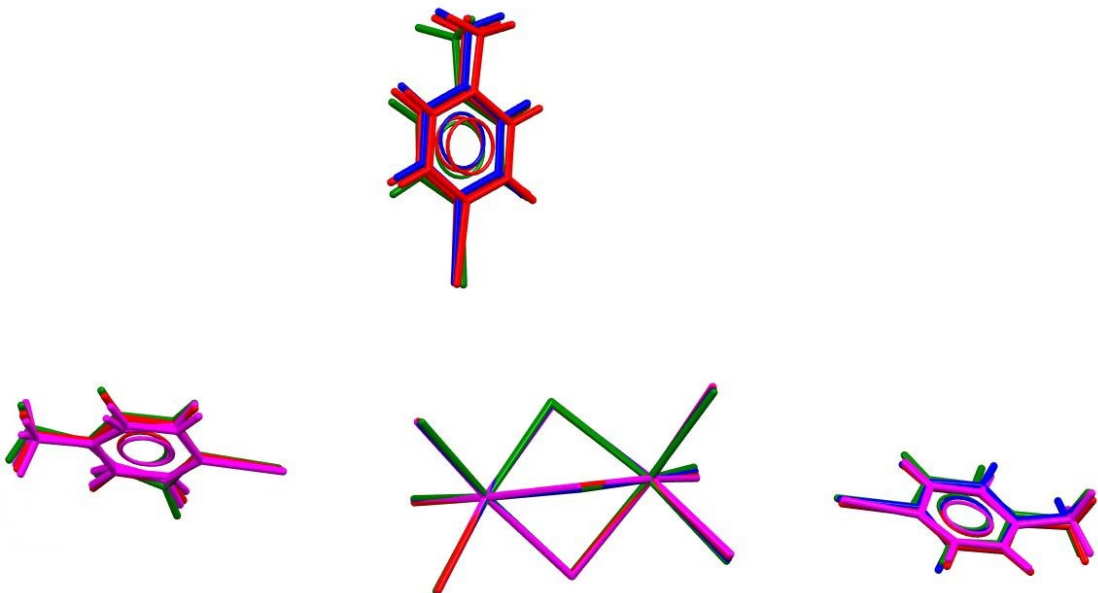


Figure S9. The structural overlay of **C\_2** at 100 K (blue), 250 K (green), 296 K (purple) and 350 K (red). The  $\text{Bi}_2\text{I}_9^{3-}$  anions are almost identical at variant temperatures.

Table S2. The geometric information for the  $\text{Bi}_2\text{I}_9^{3-}$  species and the halogen bonding interactions in **C\_2** at variant temperatures.

	<b>100 K</b>	<b>250 K</b>	<b>296 K</b>	<b>350 K</b>
<b>Bond lengths/<math>\text{\AA}</math></b>				
<b>Bi1-I1</b>	2.997 (3)	2.989 (5)	2.9787 (9)	2.977 (6)
<b>Bi1-I2</b>	2.9575(19)	2.942 (4)	2.9588 (9)	2.962 (5)
<b>Bi1-I3</b>	2.9226 (18)	2.905 (4)	2.9257 (8)	2.921 (5)
<b>Bi1-I4</b>	3.2488 (19)	3.259 (4)	3.2533 (8)	3.268 (5)
<b>Bi1-I5</b>	3.2314 (19)	3.231 (4)	3.2380 (9)	3.236 (5)
<b>Bi1-I6</b>	3.178 (2)	3.188 (5)	3.2014 (8)	3.216 (5)
<b>Bi2-I4</b>	3.294 (2)	3.294 (4)	3.2933 (8)	3.294 (4)
<b>Bi2-I5</b>	3.2048 (19)	3.223 (4)	3.2417 (9)	3.260 (5)
<b>Bi2-I6</b>	3.251 (2)	3.247 (5)	3.2481 (8)	3.237 (5)
<b>Bi2-I7</b>	2.953 (2)	2.955 (5)	2.9547 (8)	2.958 (5)
<b>Bi2-I8</b>	2.9582 (19)	2.941 (4)	2.9475 (9)	2.934 (5)
<b>Bi2-I9</b>	2.928 (2)	2.916 (4)	2.9289 (8)	2.940 (6)
<b>I1-Bi1-I4</b>	89.79 (6)	89.35 (13)	89.02 (3)	88.62 (15)
<b>Bond angles/<math>^\circ</math></b>				
<b>I1-Bi1-I5</b>	93.80 (6)	93.31 (14)	93.45 (2)	93.66 (15)
<b>I1-Bi1-I6</b>	174.53 (7)	173.65 (14)	173.18 (2)	172.42 (16)
<b>I2-Bi1-I1</b>	93.76 (7)	93.84 (14)	93.87 (3)	94.05 (16)
<b>I2-Bi1-I4</b>	91.97 (5)	91.65 (11)	91.794 (19)	92.18 (12)
<b>I2-Bi1-I5</b>	170.80 (6)	170.60 (12)	170.54 (2)	170.20 (13)
<b>I2-Bi1-I6</b>	90.40 (6)	90.60 (12)	90.46 (2)	90.05 (14)
<b>I3-Bi1-I1</b>	92.58 (6)	92.89 (14)	93.29 (3)	93.72 (16)
<b>I3-Bi1-I2</b>	93.92 (6)	93.57 (13)	92.93 (2)	92.66 (14)
<b>I3-Bi1-I4</b>	173.49 (6)	174.17 (11)	174.59 (2)	174.46 (13)
<b>I3-Bi1-I5</b>	90.97 (5)	92.16 (12)	92.62 (2)	92.87 (13)
<b>I3-Bi1-I6</b>	90.67 (6)	91.37 (13)	91.74 (3)	92.46 (15)
<b>I5-Bi1-I4</b>	82.82 (5)	82.32 (10)	82.353 (17)	81.96 (11)
<b>I6-Bi1-I4</b>	86.52 (5)	85.97 (11)	85.57 (2)	84.84 (13)
<b>I6-Bi1-I5</b>	81.75 (5)	81.82 (11)	81.72 (2)	81.63 (12)
<b>I5-Bi2-I4</b>	82.52 (5)	81.90 (10)	81.682 (19)	81.21 (11)
<b>I5-Bi2-I6</b>	81.03 (5)	81.04 (11)	80.957 (19)	84.10 (12)

<b>I6-Bi2-I4</b>	84.58 (5)	84.46 (11)	84.18 (2)	80.94 (12)
<b>I7-Bi2-I4</b>	87.86 (6)	89.23 (12)	90.46 (2)	91.47 (13)
<b>I7-Bi2-I5</b>	93.98 (6)	93.03 (12)	92.77 (2)	92.13 (13)
<b>I7-Bi2-I6</b>	171.42 (7)	171.87 (12)	172.26 (2)	172.26 (14)
<b>I7-Bi2-I8</b>	94.30 (6)	90.44 (11)	89.79 (2)	89.26 (13)
<b>I8-Bi2-I4</b>	91.14 (5)	169.41 (12)	169.14 (2)	168.83 (13)
<b>I8-Bi2-I5</b>	169.37 (6)	91.00 (12)	91.54 (2)	92.36 (14)
<b>I8-Bi2-I6</b>	89.91 (5)	94.17 (13)	94.03 (2)	93.94 (14)
<b>I9-Bi2-I4</b>	175.11 (5)	174.93 (12)	174.93 (2)	94.54 (15)
<b>I9-Bi2-I5</b>	92.63 (5)	93.27 (12)	93.89 (2)	174.59 (14)
<b>I9-Bi2-I6</b>	94.03 (6)	93.30 (13)	92.72 (3)	94.60 (14)
<b>I9-Bi2-I7</b>	93.17 (6)	92.58 (12)	92.22 (3)	91.89 (15)
<b>I9-Bi2-I8</b>	93.55(6)	94.15 (12)	94.31 (2)	92.11 (14)
<b>XBs</b>				
I1O...I2	3.811 (4)	3.812 (5)	3.825 (9)	3.820 (7)
I2OA...I3	3.701 (4)	3.799 (6)	3.964 (9)	3.980 (7)
I3O...I8	3.764 (4)	3.818 (6)	3.877 (9)	3.910 (7)

- Other characterizations

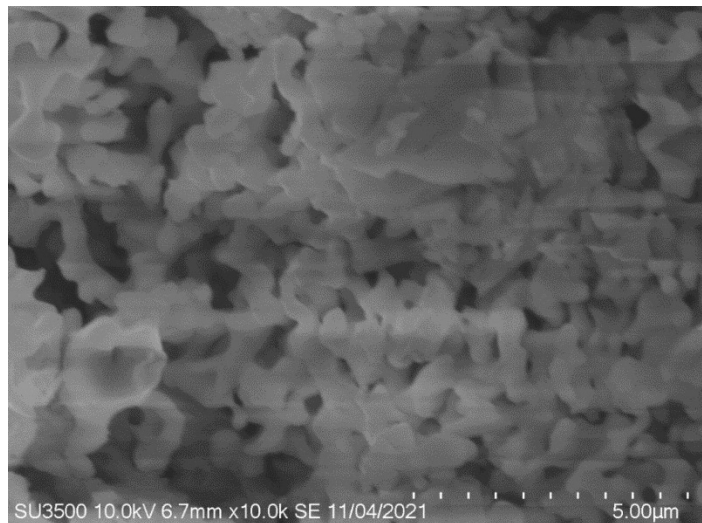


Figure S10. The SEM picture for the amorphous product **P\_1**.



Figure S11. The SEM picture for **C\_1**.

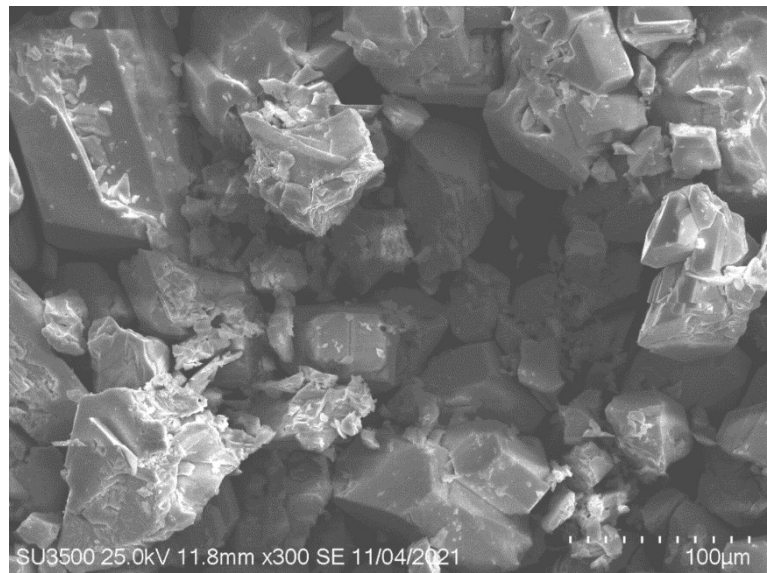


Figure S12. The SEM picture for C\_2.

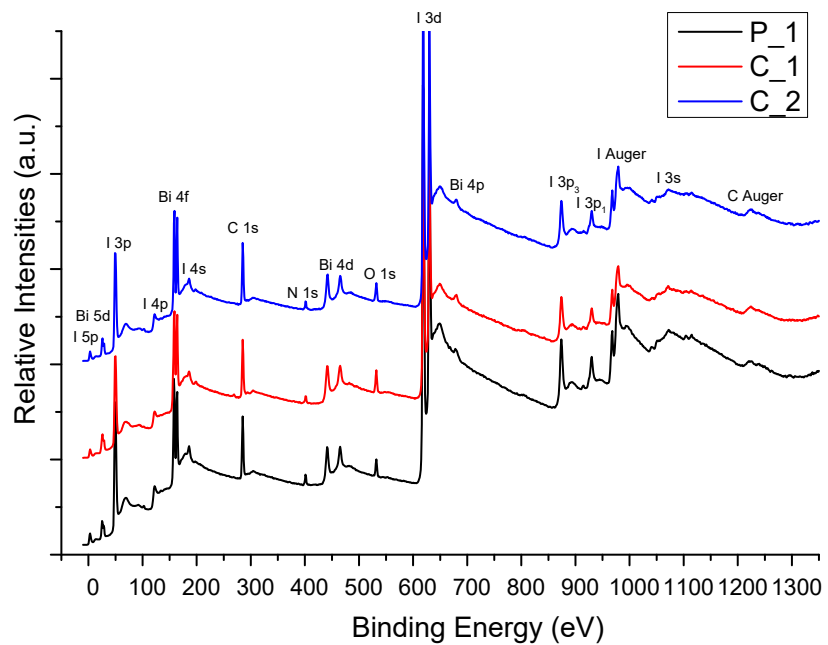


Figure S13. The full spectroscopy of the X-ray photoelectron binding energy for P\_1, C\_1 and C\_2. They show very similar signals indicate the components and bonding are similar.

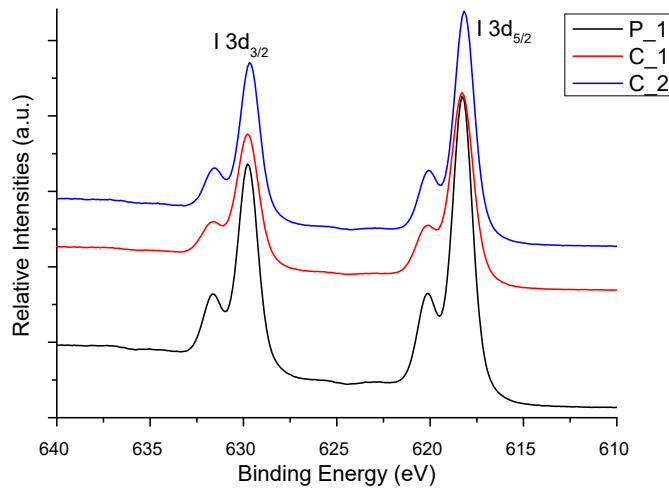


Figure S14. The I  $3d_{3/2}$  and I  $3d_{5/2}$  signals at 629.79 eV and 618.28 eV, respectively. The small peaks at 631.68 eV and 620.08 eV indicate the existence of less negatively charged iodide in the structures.

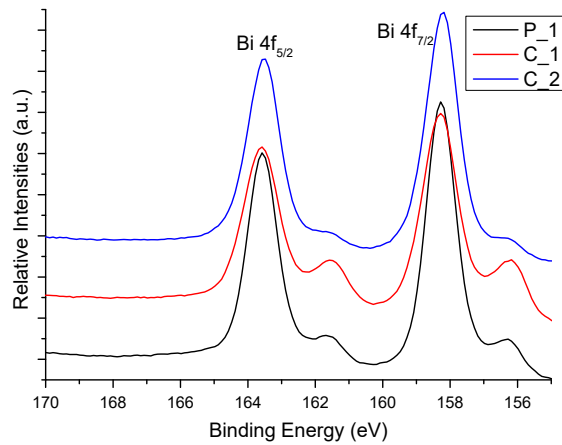


Figure S15. The Bi  $4f_{7/2}$  and Bi  $4f_{5/2}$  signals at 158.28 eV and 163.58 eV, respectively. The small peaks at 156.28 eV and 161.58 eV indicate the existence of low valence Bismuth species in the structures.

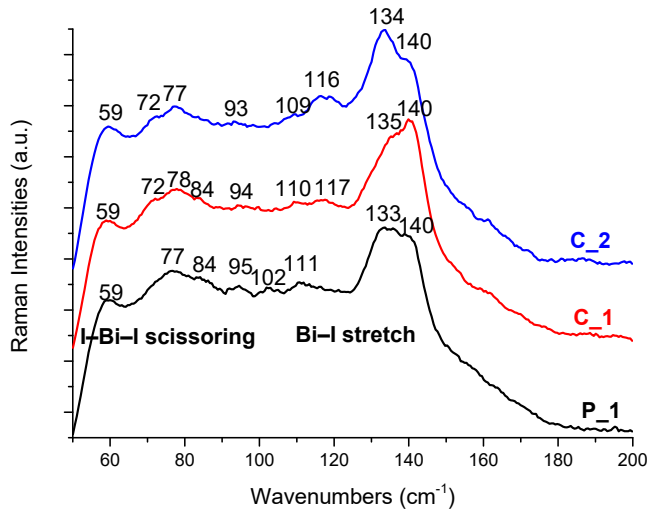


Figure S16. Raman spectroscopy of **P\_1**, **C\_1** and **C\_2**. The signals were assigned according to literatures [9].

- **Theoretical computations**

The initial models of **C\_2** and **C\_3** were taken from the X-ray crystallography data using one set of disorder structure. For the initial model of **C\_1**, intercept  $[\text{Bi}_2\text{I}_9]^{3-}$  and  $[\text{Bi}\text{I}_6]^{3-}$  fragments from two 1D  $[\text{Bi}\text{I}_4]$  chain and select the surrounding organic cations to maintain the electrical neutrality of the system.

DFT calculations were carried out by Gaussian 09 software [10]. Double zeta valence quality plus polarization basis set Jorge-DZP-DKH with  $\omega\text{B}97\text{XD}$  method was used for single point calculation.[11] The calculation results are used for Bader's Quantum Theory Atoms-in-Molecules(QTAIM) [12] analysis.

The QTAIM analysis and the localized orbital locator (LOL) [13] isosurface diagrams were carried out with Multiwfn [14].

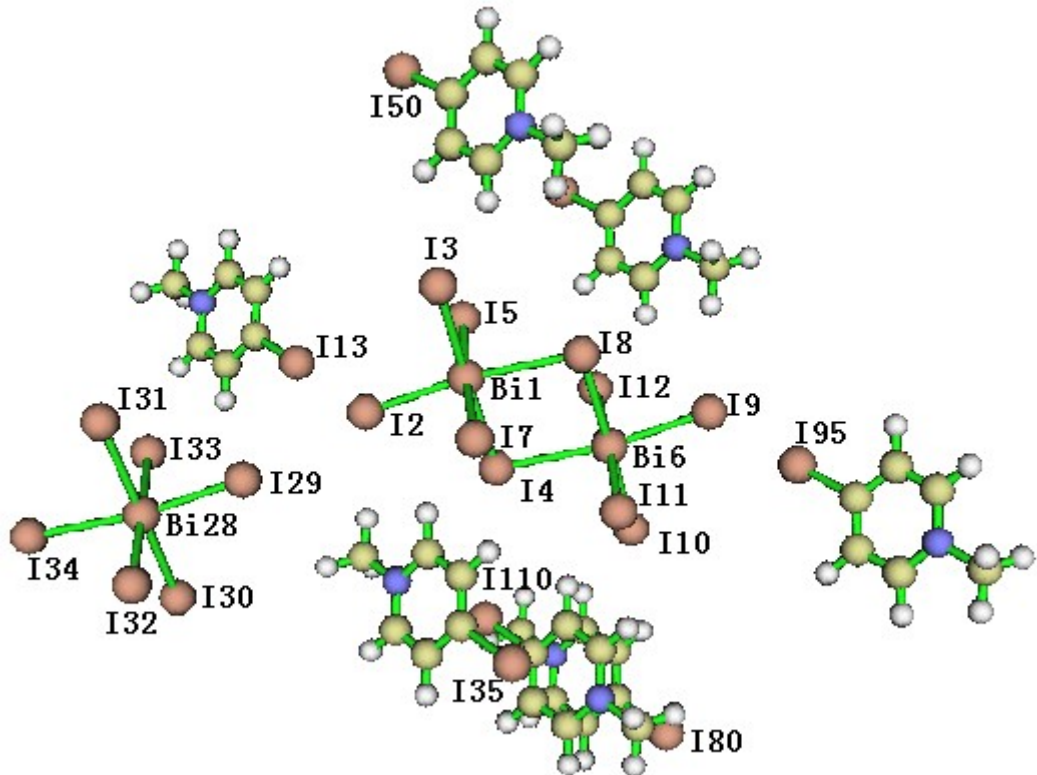


Figure S17. The structural model and atomic labels for the DFT computations in **C\_1**.

The atomic coordinates of **C\_1**

Bi	4.020000	13.274000	10.043000
I	2.871000	10.580000	10.229000
I	1.452000	14.510000	8.855000
I	6.549000	12.173000	11.453000
I	5.106000	12.967000	7.335000
Bi	7.817000	15.162000	11.764000
I	2.652000	13.927000	12.951000
I	5.288000	16.263000	10.353000
I	8.966000	17.856000	11.577000
I	10.384000	13.927000	12.951000
I	6.730000	15.469000	14.472000
I	9.185000	14.510000	8.855000
I	3.038000	8.469000	7.320000
N	2.913000	5.513000	3.506000
C	3.000000	7.199000	5.658000
C	2.723000	7.694000	4.412000
H	2.550000	8.753000	4.270000
C	2.666000	6.819000	3.330000
H	2.423000	7.194000	2.344000
C	3.199000	4.995000	4.709000
H	3.397000	3.935000	4.812000

C	3.240000	5.817000	5.816000
H	3.454000	5.408000	6.795000
C	2.847000	4.612000	2.319000
H	2.150000	3.827000	2.507000
H	3.810000	4.195000	2.135000
H	2.532000	5.169000	1.467000
Bi	-0.158000	4.801000	11.764000
I	0.991000	7.495000	11.577000
I	2.410000	3.565000	12.951000
I	-2.687000	5.902000	10.353000
I	-1.244000	5.108000	14.472000
I	1.211000	4.148000	8.855000
I	-1.425000	1.812000	11.453000
I	4.849000	12.326000	18.223000
N	4.723000	9.370000	14.410000
C	4.810000	11.055000	16.561000
C	4.533000	11.551000	15.316000
H	4.360000	12.610000	15.173000
C	4.477000	10.675000	14.233000
H	4.233000	11.051000	13.247000
C	5.009000	8.852000	15.612000
H	5.208000	7.792000	15.715000
C	5.050000	9.674000	16.719000
H	5.264000	9.265000	17.698000
C	4.657000	8.468000	13.222000
H	3.960000	7.684000	13.410000
H	5.621000	8.052000	13.038000
H	4.342000	9.026000	12.370000
I	-0.745000	16.111000	3.583000
N	-0.619000	19.066000	7.397000
C	-0.706000	17.381000	5.245000
C	-0.430000	16.886000	6.491000
H	-0.256000	15.826000	6.633000
C	-0.373000	17.761000	7.573000
H	-0.129000	17.385000	8.559000
C	-0.905000	19.584000	6.194000
H	-1.104000	20.644000	6.091000
C	-0.947000	18.762000	5.087000
H	-1.160000	19.171000	4.108000
C	-0.553000	19.968000	8.584000
H	0.143000	20.753000	8.396000

H	-1.517000	20.384000	8.768000
H	-0.238000	19.410000	9.436000
I	6.988000	16.111000	3.583000
N	7.114000	19.066000	7.397000
C	7.026000	17.381000	5.245000
C	7.303000	16.886000	6.491000
H	7.477000	15.826000	6.633000
C	7.360000	17.761000	7.573000
H	7.604000	17.385000	8.559000
C	6.828000	19.584000	6.194000
H	6.629000	20.644000	6.091000
C	6.786000	18.762000	5.087000
H	6.573000	19.171000	4.108000
C	7.180000	19.968000	8.584000
H	7.876000	20.753000	8.396000
H	6.216000	20.384000	8.768000
H	7.495000	19.410000	9.436000
I	12.582000	12.326000	18.223000
N	12.456000	9.370000	14.410000
C	12.543000	11.055000	16.561000
C	12.266000	11.551000	15.316000
H	12.093000	12.610000	15.173000
C	12.209000	10.675000	14.233000
H	11.966000	11.051000	13.247000
C	12.742000	8.852000	15.612000
H	12.940000	7.792000	15.715000
C	12.783000	9.674000	16.719000
H	12.997000	9.265000	17.698000
C	12.390000	8.468000	13.222000
H	11.693000	7.684000	13.410000
H	13.354000	8.052000	13.038000
H	12.075000	9.026000	12.370000
I	8.798000	19.968000	14.486000
N	8.924000	22.923000	18.300000
C	8.837000	21.238000	16.149000
C	9.114000	20.743000	17.394000
H	9.287000	19.683000	17.536000
C	9.170000	21.618000	18.476000
H	9.414000	21.242000	19.462000
C	8.638000	23.441000	17.097000
H	8.439000	24.501000	16.994000

C	8.597000	22.619000	15.990000
H	8.383000	23.028000	15.011000
C	8.990000	23.825000	19.487000
H	9.686000	24.610000	19.299000
H	8.026000	24.241000	19.671000
H	9.305000	23.267000	20.339000
I	8.557000	9.606000	14.486000
N	8.682000	12.562000	18.300000
C	8.595000	10.877000	16.149000
C	8.872000	10.381000	17.394000
H	9.045000	9.322000	17.536000
C	8.929000	11.257000	18.476000
H	9.172000	10.881000	19.462000
C	8.396000	13.080000	17.097000
H	8.198000	14.140000	16.994000
C	8.355000	12.258000	15.990000
H	8.141000	12.667000	15.011000
C	8.748000	13.464000	19.487000
H	9.445000	14.248000	19.299000
H	7.785000	13.880000	19.671000
H	9.063000	12.906000	20.339000

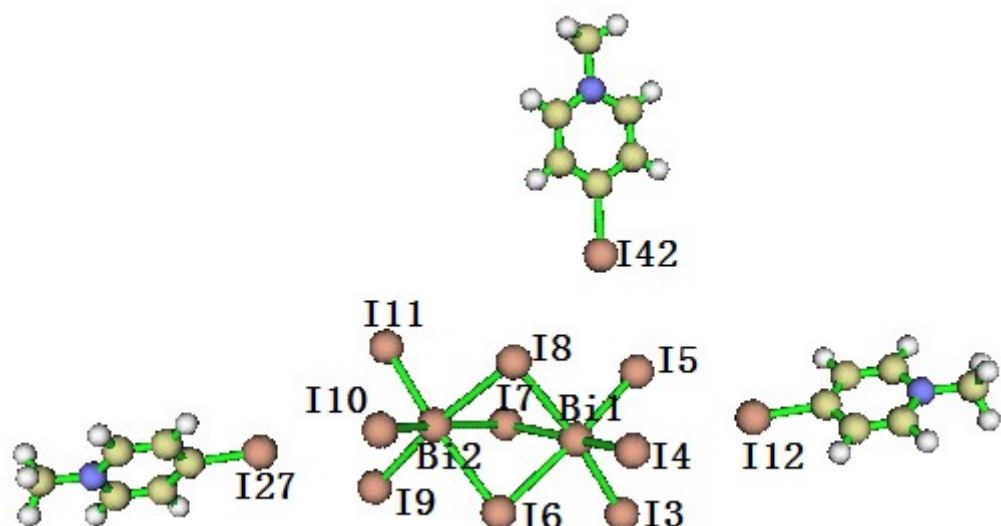


Figure S18. The structural model and atomic labels for the DFT computations in **C\_2**.

#### The atomic coordinates of **C\_2**

Bi	11.235844	12.614540	12.489070
Bi	8.460736	9.495512	12.089068
I	11.438034	14.880475	10.567059
I	14.144839	12.073537	12.464070

I	11.428783	14.360639	14.829083
I	10.736903	10.603434	9.983056
I	7.999829	12.674542	12.525070
I	10.747646	10.041601	14.330080
I	6.470840	9.359426	9.908055
I	9.419661	6.741483	11.662065
I	6.472589	8.727587	14.099079
I	15.551876	15.239614	14.085079
N	19.030911	18.115690	15.720088
C	17.061889	16.482648	14.835083
C	18.323921	16.387627	14.295080
H	18.545936	15.654594	13.530076
C	19.274932	17.228648	14.739082
H	20.261960	17.189630	14.296080
C	17.811880	18.228711	16.248091
H	17.613865	18.961744	17.020095
C	16.820869	17.407690	15.806088
H	15.827844	17.490707	16.230091
C	20.098927	19.017710	16.133090
H	20.898887	18.450724	16.551092
H	19.725911	19.699741	16.862094
H	20.451995	19.559679	15.286085
I	6.128659	5.175425	10.351058
N	4.173580	1.063348	8.806049
C	5.284626	3.424392	9.678054
C	5.768559	2.212404	10.111056
H	6.604525	2.178430	10.799060
C	5.201537	1.056382	9.677054
H	5.583484	0.110392	10.039056
C	3.690647	2.223334	8.323046
H	2.863681	2.223307	7.623043
C	4.249672	3.390354	8.718049
H	3.893728	4.318341	8.289046
C	3.503552	-0.187673	8.407047
H	4.184519	-1.001673	8.509048
H	3.188608	-0.113712	7.391041
H	2.656508	-0.351649	9.031050
I	11.355528	12.060750	17.932100
N	11.112222	10.641924	22.551126
C	11.258396	11.459826	19.929111
C	11.599373	12.324870	20.964117

H	11.889417	13.188866	20.782116
C	11.499285	11.874918	22.261124
H	11.710270	12.455948	22.955128
C	10.833239	9.755883	21.601121
H	10.589194	8.884888	21.814122
C	10.908327	10.168834	20.283113
H	10.727340	9.554805	19.610110
C	10.931130	10.255978	23.962134
H	10.044119	10.488990	24.246135
H	11.573120	10.717001	24.506137
H	11.056090	9.307977	24.054134

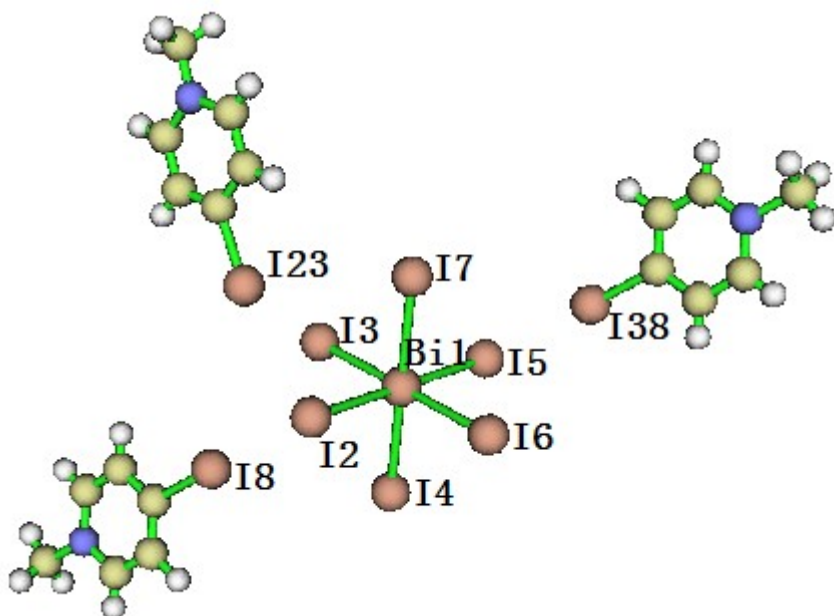


Figure S19. The structural model and atomic labels for the DFT computations in **C\_3**.

#### The atomic coordinates of **C\_3**

Bi	4.573581	13.541938	6.092966
I	7.589623	12.901941	5.623968
I	4.488429	11.344948	8.224954
I	3.741733	11.513948	3.916978
I	1.558538	14.181935	6.562963
I	4.658732	15.738928	3.961978
I	5.405428	15.569929	8.269953
I	7.761628	9.353957	5.565969
N	8.151648	4.548979	5.299970
C	7.947635	7.266967	5.469969
C	8.068554	6.499970	6.620963
H	8.091494	6.907969	7.456958

C	8.153562	5.144977	6.513963
H	8.215507	4.623979	7.281959
C	8.036727	5.278976	4.186976
H	8.029785	4.852978	3.360981
C	7.928723	6.629970	4.239976
H	7.829787	7.206967	3.327981
C	8.292652	3.058986	5.244970
H	7.584688	2.689988	4.711973
H	8.243589	2.699988	6.133965
H	9.139682	2.831987	4.854973
I	8.644378	12.956941	9.109949
C	9.206208	14.573934	11.528935
H	9.167252	15.267931	10.911938
C	9.041238	13.258940	11.105937
C	9.098172	12.219944	12.028932
H	8.988192	11.341948	11.744934
C	9.322077	12.494943	13.371924
H	9.361034	11.800946	13.988921
N	9.487048	13.809937	13.793922
C	9.429113	14.848932	12.872927
H	9.540093	15.726928	13.154926
C	9.624954	14.079936	15.111915
H	10.508946	14.426934	15.273914
H	9.502918	13.274940	15.618912
H	8.974934	14.730933	15.376913
I	1.385533	17.729919	6.620963
N	0.996513	22.534897	6.886961
C	1.200526	19.816910	6.716962
C	1.078607	20.583906	5.565969
H	1.056667	20.175908	4.729973
C	0.993600	21.938900	5.672968
H	0.932654	22.459898	4.904972
C	1.111434	21.804901	7.999955
H	1.117376	22.230899	8.825950
C	1.218439	20.453907	7.946955
H	1.317374	19.876910	8.858950
C	0.855509	24.024891	6.941961
H	1.562473	24.393889	7.474958
H	0.904572	24.383889	6.052966
H	0.008479	24.251890	7.331959

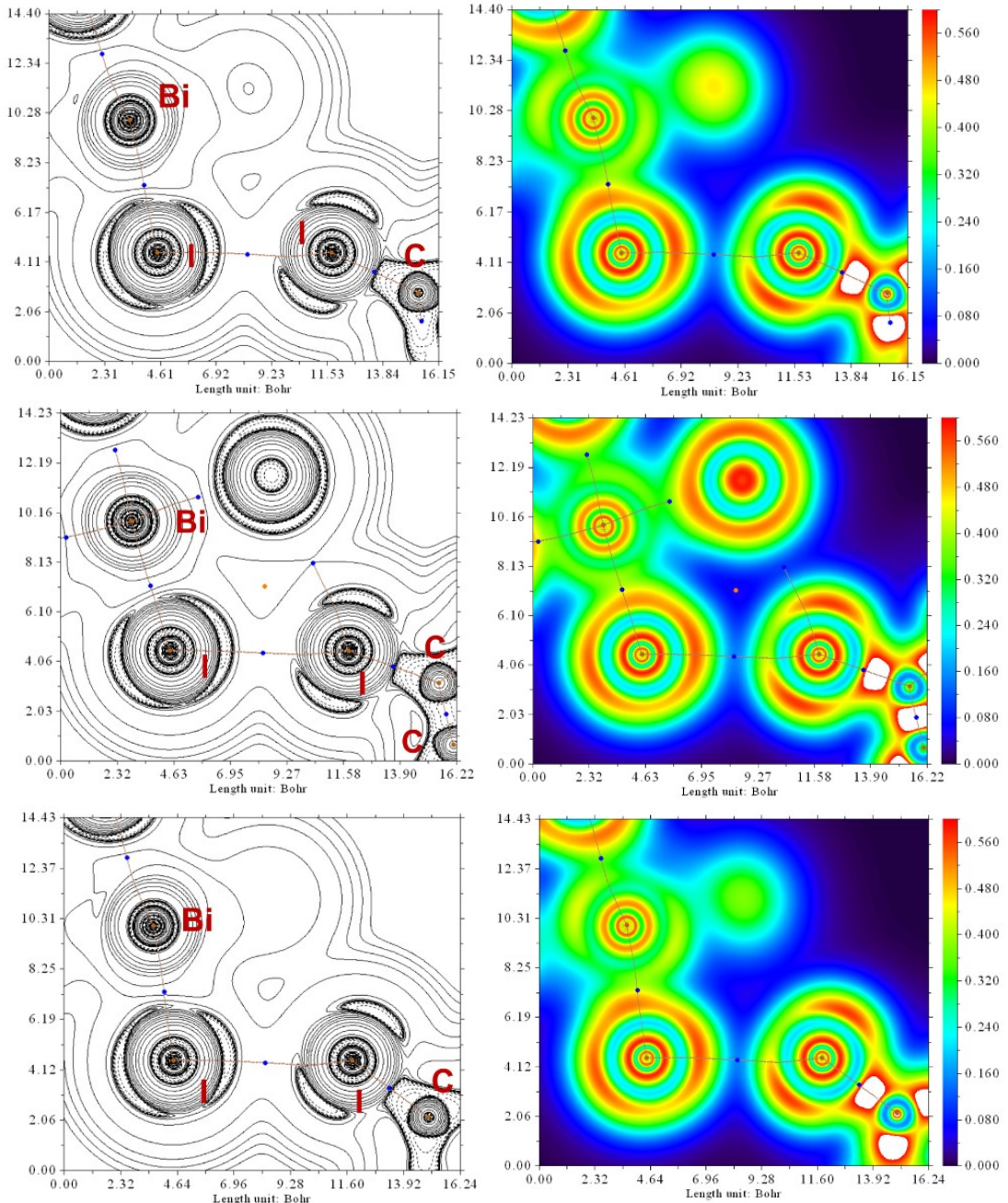


Figure S20. The Laplacian of the electron density distribution (left) and the LOL pictures (right) for the C1-I1O···I2-Bi1 (top), C7A-I2OA···I3-Bi1 (middle), and C13-I3O···I8-Bi2 (bottom) in **C<sub>2</sub>**.

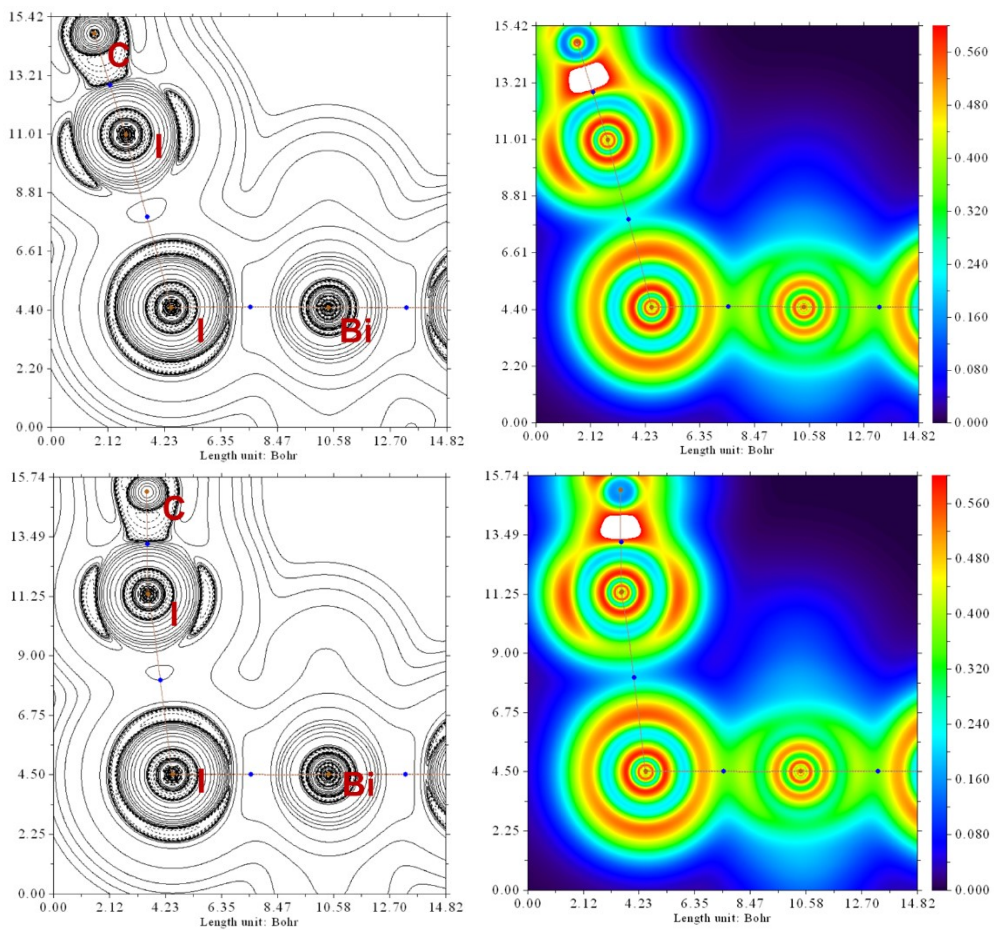


Figure S21. The Laplacian of the electron density distribution (left) and the LOL pictures (right) for C7-I2O···I1-Bi1 (top) C1-I1O···I1-Bi1 (bottom) in **C\_3**.

Table S3. Values of the properties at the bcp's in a.u. including the electron densities  $\rho(r)$ , Laplacian of the electron density  $\nabla^2\rho(r)$  and energy density  $H_b$ , as well as the AIM charges for Bi and I in **C\_1**, **C\_2** and **C\_3**.

	<b>Bonds</b>	$\rho(r)$	$\nabla^2\rho(r)$	$H(r)$	<b>AIM charges</b>	
					<b>Bi</b>	<b>I</b>
<b>C_1</b>	Bi1-I2	0.051	0.075	-0.013	1.31	-0.60
	Bi1-I5	0.050	0.048	-0.012	1.31	-0.50
	Bi6-I9	0.051	0.083	-0.013	1.30	-0.71
	Bi6-I11	0.050	0.052	-0.012	1.30	-0.53
	Bi1-I8	0.032	0.064	-0.005	1.31	-0.59
	Bi1-I4	0.040	0.053	-0.008	1.31	-0.58
	Bi6-I4	0.033	0.067	-0.005	1.30	-0.58
	Bi6-I8	0.039	0.053	-0.007	1.30	-0.59
<b>C_2</b>	Bi1-I3	0.048	0.044	-0.011	1.37	-0.46
	Bi1-I4	0.050	0.050	-0.012	1.37	-0.49
	Bi1-I5	0.052	0.056	-0.014	1.37	-0.52
	Bi2-I9	0.050	0.054	-0.013	1.34	-0.51
	Bi2-I10	0.051	0.050	-0.013	1.34	-0.49
	Bi2-I11	0.052	0.048	-0.013	1.34	-0.48
	Bi1-I6	0.033	0.049	-0.005	1.37	-0.53
	Bi1-I7	0.034	0.048	-0.005	1.37	-0.52
	Bi1-I8	0.035	0.048	-0.006	1.37	-0.55
	Bi2-I6	0.030	0.044	-0.004	1.34	-0.53
<b>C_3</b>	Bi2-I7	0.033	0.048	-0.005	1.34	-0.52
	Bi2-I8	0.033	0.053	-0.005	1.34	-0.55
	Bi1-I2	0.040	0.058	-0.008	1.49	-0.60
	Bi1-I3	0.042	0.043	-0.008	1.49	-0.53
	Bi1-I4	0.041	0.039	-0.008	1.49	-0.51
	Bi1-I5	0.040	0.058	-0.008	1.49	-0.61
	Bi1-I6	0.042	0.041	-0.008	1.49	-0.51
	Bi1-I7	0.040	0.043	-0.008	1.49	-0.55

Table S4. The bonding indicators including the Meyer Bond Order (MBO), Fuzzy Bond Order (FBO), Laplacian Bond Order (LBO), and Intrinsic Bond Strength Index (IBSI) at the bcp's in **C\_1**, **C\_2** and **C\_3**.

	<b>Bonds</b>	<b>LBO</b>	<b>FBO</b>	<b>MBO</b>	<b>IBSI</b>
<b>C_1</b>	Bi1-I2	0.023	0.92	0.25	0.18
	Bi1-I5	0.023	1.12	0.72	0.16
	Bi6-I9	0.033	0.94	0.12	0.19
	Bi6-I11	0.024	1.09	0.66	0.17
	Bi1-I8	0.022	0.58	0.08	0.11
	Bi1-I4	0.014	0.85	0.49	0.12

	Bi6-I4	0.017	0.57	0.06	0.11
	Bi6-I8	0.023	0.85	0.51	0.12
<b>C_2</b>	Bi1-I3	0.023	1.09	0.68	0.15
	Bi1-I4	0.022	1.04	0.59	0.16
	Bi1-I5	0.024	1.03	0.51	0.16
	Bi2-I9	0.025	1.05	0.54	0.15
	Bi2-I10	0.023	1.07	0.62	0.17
	Bi2-I11	0.026	1.13	0.67	0.17
	Bi1-I6	0.020	0.65	0.31	0.090
	Bi1-I7	0.020	0.67	0.35	0.094
	Bi1-I8	0.020	0.70	0.40	0.098
	Bi2-I6	0.020	0.65	0.39	0.085
	Bi2-I7	0.021	0.67	0.34	0.094
	Bi2-I8	0.020	0.61	0.24	0.090
<b>C_3</b>	Bi1-I2	0.018	0.70	0.17	0.11
	Bi1-I3	0.018	0.97	0.65	0.12
	Bi1-I4	0.018	0.98	0.68	0.13
	Bi1-I5	0.021	0.73	0.20	0.11
	Bi1-I6	0.019	0.99	0.67	0.12
	Bi1-I7	0.018	0.94	0.63	0.13

Table S5. Values of the electron densities  $\rho(r)$ , Laplacian of the electron density  $\nabla^2\rho(r)$ , energy density  $H_b$ , potential energy density  $V(r)$  (a.u.), Lagrangian kinetic energy  $G(r)$  (a.u.) at the bcps for the Bi-I-C interactions in **C\_1**, **C\_2** and **C\_3**, bond lengths  $l$  ( $\text{\AA}$ ), rationalized bonding parameter  $R$  ( $R = l/2r_{\text{vdw}(I)}$ ) LBO, MBO, IBSI, as well as energies  $E_{\text{int}}$  ( $\text{kJ}\cdot\text{mol}^{-1}$ ) defined by different approaches.

Contacts	$\rho(r)$	$\nabla^2\rho(r)$	$H_b$	$V(r)$	$G(r)$	LBO	MBO	IBSI	$E_{\text{int}}^a$	$E_{\text{int}}^b$	$l$	$R$
<b>C_1</b>												
I2···I29	0.010	0.030	0.0011	-0.005	0.006	0.004	0.13	0.029	8.9	10.6	3.856	0.97
I2···I13	0.015	0.039	0.00042	-0.009	0.009	0.012	0.22	0.044	16.1	15.8	3.598	0.91
<b>C-2</b>												
I12···I4	0.010	0.033	0.001	-0.006	0.007	0.011	0.11	0.034	10.7	12.3	3.825	0.97
I42···I5	0.009	0.031	0.001	-0.005	0.006	0.010	0.12	0.031	8.9	10.6	3.863	0.98
I27···I10	0.010	0.032	0.001	-0.006	0.007	0.012	0.08	0.031	10.7	12.3	3.873	0.98
<b>C-3</b>												
I2···I8	0.017	0.042	0.000	-0.010	0.010	0.018	0.21	0.054	17.9	17.6	3.553	0.90
I2···I23	0.014	0.040	0.001	-0.009	0.009	0.014	0.17	0.047	16.1	15.8	3.643	0.92
I5···I38	0.017	0.041	0.000	-0.010	0.010	0.019	0.25	0.054	17.9	17.6	3.553	0.90

$$E_{\text{int}}^a = 0.68(-V(r)); E_{\text{int}}^b = 0.67G(r) [15].$$

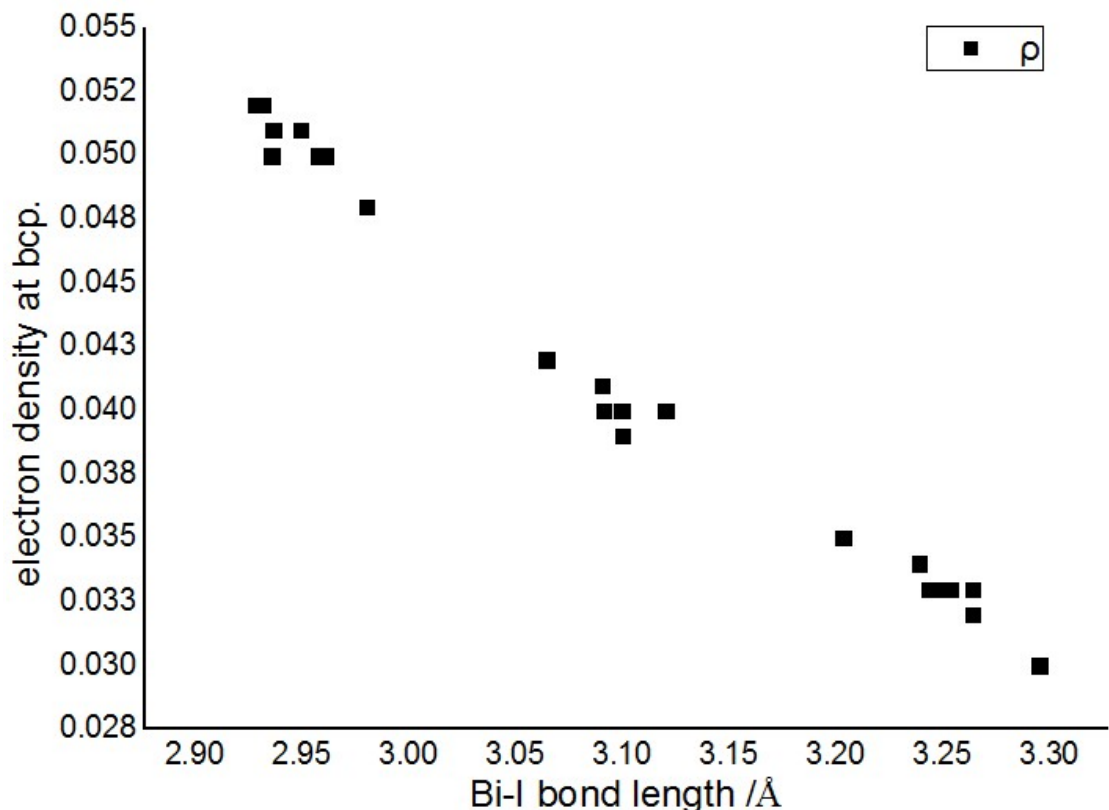


Figure S22. The plots showing Bi-I bond lengths and electron density at bond critical points relationship.

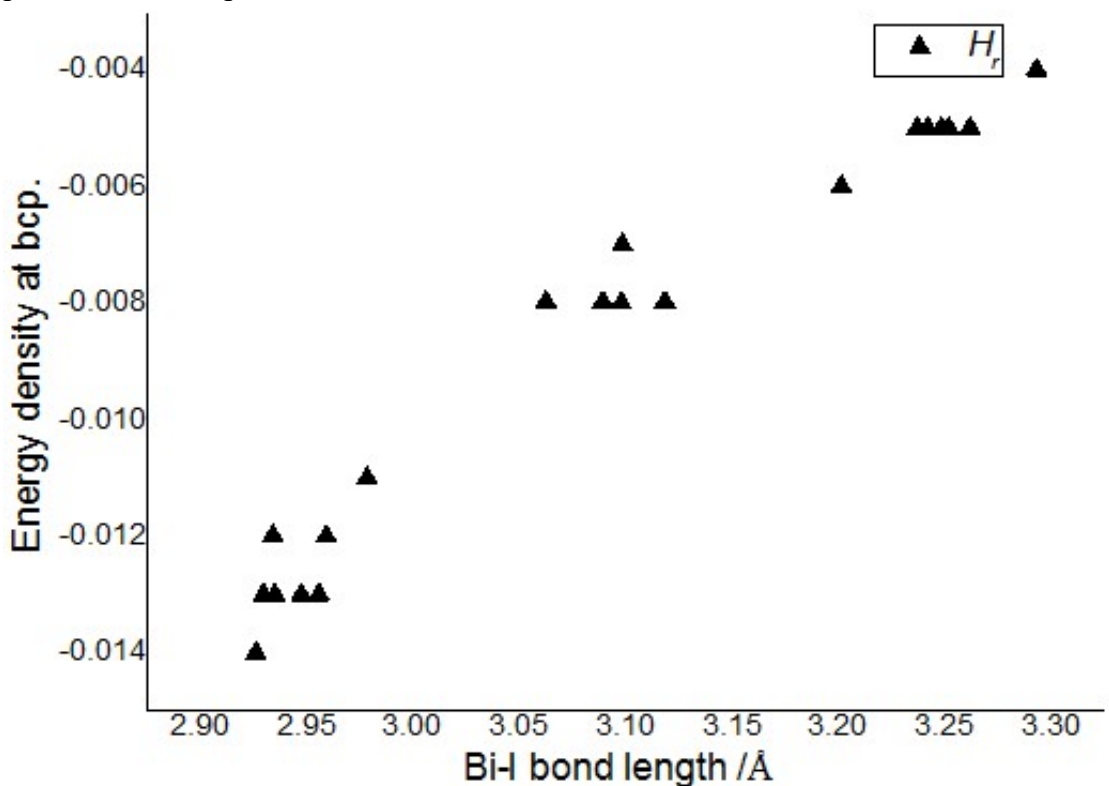


Figure S23. The plots showing Bi-I bond lengths and energy density at bond critical points relationship.

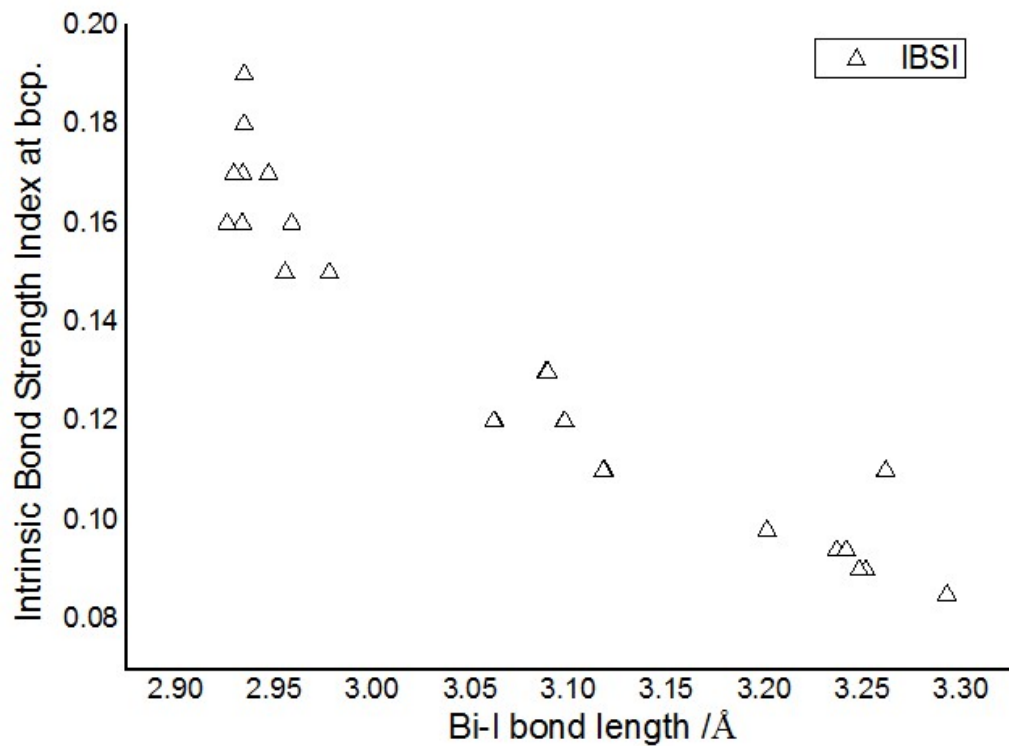


Figure S24. The plots showing Bi-I bond lengths and IBSI at bond critical points relationship.

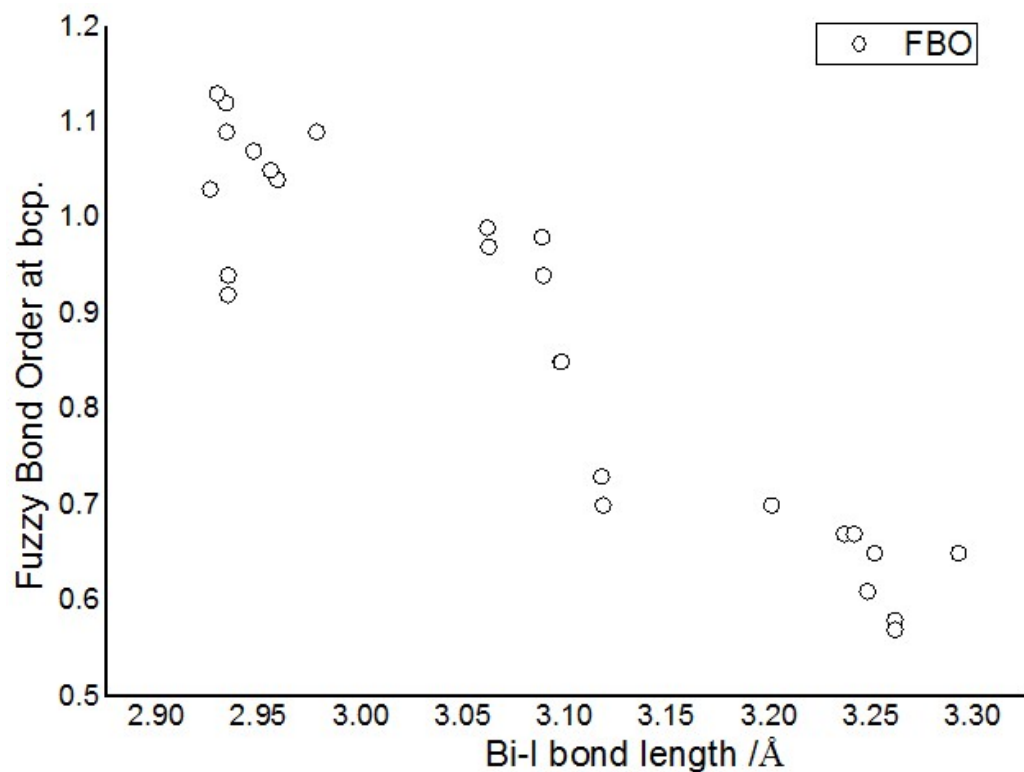


Figure S25. The plots showing Bi-I bond lengths and FBO at bond critical points relationship.

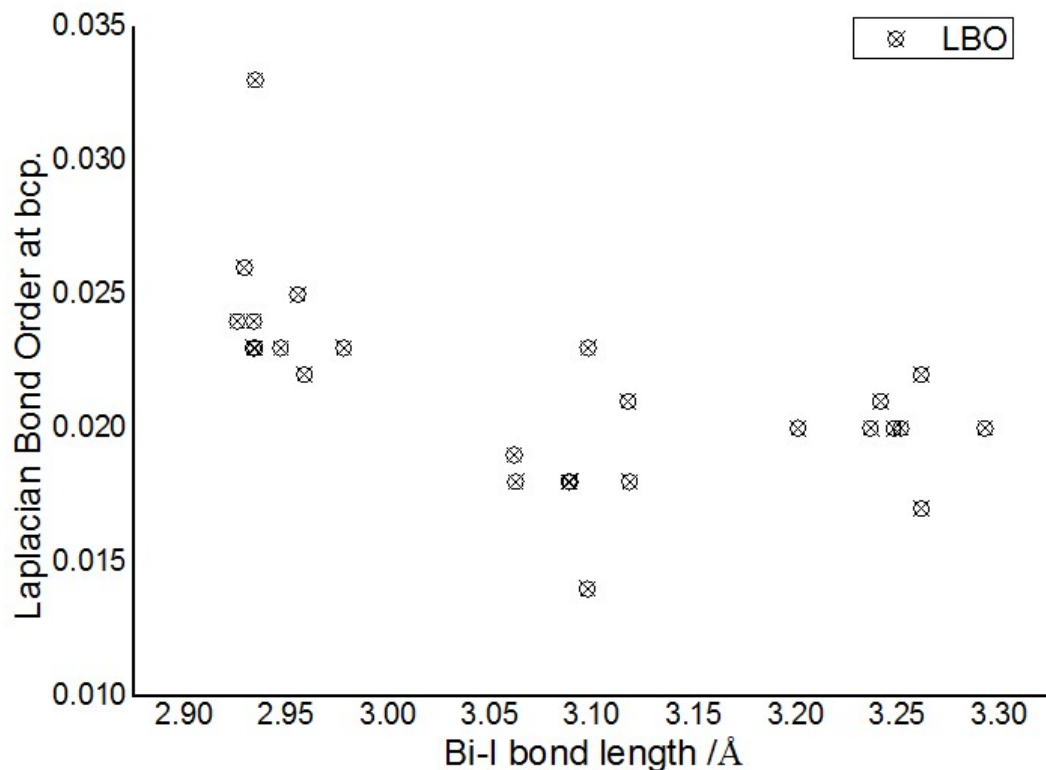


Figure S26. The plots showing Bi-I bond lengths and LBO values at bond critical points relationship.

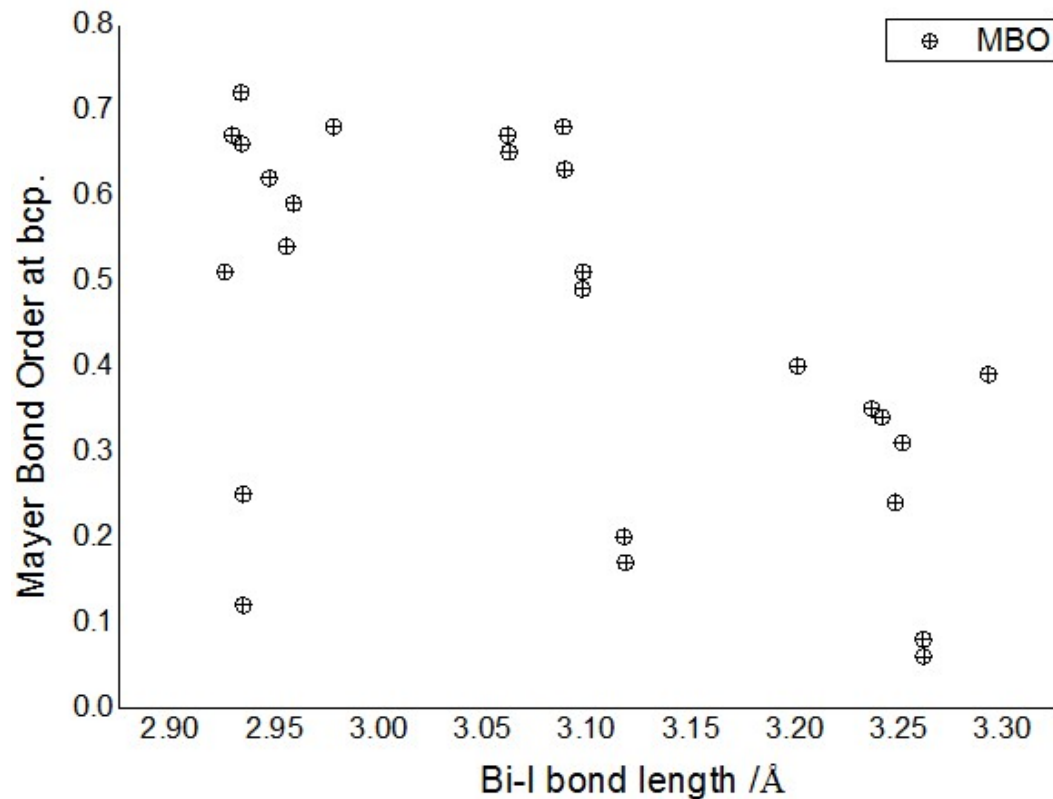


Figure S27. The plots showing Bi-I bond lengths and MBO values at bond critical points relationship.

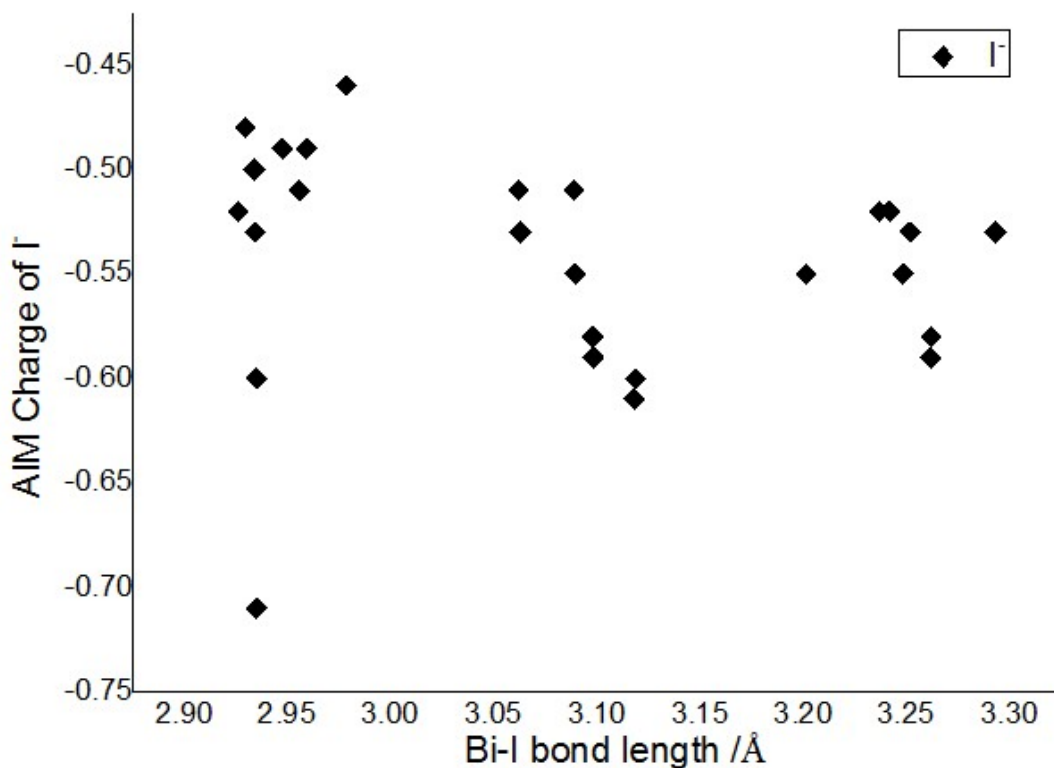


Figure S28. The plots showing Bi-I bond lengths and the AIM charges for I<sup>-</sup> at bond critical points relationship.

### References:

1. J. E. Reeve, H. A. Collins, K. De Mey, M. M. Kohl, K. J. Thorley, O. Paulsen, K. Clays, H. L. Anderson, *J. Am. Chem. Soc.*, 2009, **131**, 2758-2759.
2. Bruker AXS Inc., 5465 East Cheryl Parkway, Madison, WI 53711, 2016.
3. Sheldrick, G.M. SADABS, Program for Empirical Absorption Correction of Area Detector Data. University of Gottingen, Gottingen, Germany, 2010.
4. G. M. Sheldrick, *Acta Cryst.* 2015, **A71**, 3-8.
5. O. V. Dolomanov, L. J. Bourhis, R. J. Gildea, J. A. K. Howard, H. Puschmann, *J. Appl. Cryst.*, 2009, **42**, 339–341.
6. G. M. Sheldrick, *Acta Cryst.* 2015, **C71**, 3-8.
7. D. Jayatilaka, D. J. Grimwood, A. Lee, A. Lemay, A. J. Russel, C. Taylo, S. K. Wolff, Cassam-Chenai and A. Whitton, “TONTO-A System for Computational Chemistry,” 2005
8. P. R. Spackman, M. J. Turner, J. J. McKinnon, S. K. Wolff, D. J. Grimwood, D. Jayatilaka, M. A. Spackman, *J. Appl. Cryst.*, 2021, **54**, 1006–1011.
9. J. Laane, P. W. Jagodzinski, *Inorg. Chem.*, 1980, **19**, 44-49.
10. Gaussian 09, Revision A.02, M. J. Frisch, G. W. Trucks, H. B. Schlegel, G. E. Scuseria, M. A. Robb, J. R. Cheeseman, G. Scalmani, V. Barone, G. A. Petersson, H. Nakatsuji, X. Li, M. Caricato, A. Marenich, J. Bloino, B. G. Janesko, R. Gomperts, B. Mennucci, H. P. Hratchian, J. V. Ortiz, A. F. Izmaylov, J. L. Sonnenberg, D. Williams-Young, F. Ding, F. Lipparini, F. Egidi, J. Goings, B. Peng, A. Petrone, T. Henderson, D. Ranasinghe, V. G. Zakrzewski, J. Gao, N. Rega, G. Zheng, W. Liang, M. Hada, M. Ehara, K. Toyota, R. Fukuda, J. Hasegawa, M. Ishida, T. Nakajima, Y. Honda, O. Kitao, H. Nakai, T. Vreven, K. Throssell, J. A.

- Montgomery, Jr., J. E. Peralta, F. Ogliaro, M. Bearpark, J. J. Heyd, E. Brothers, K. N. Kudin, V. N. Staroverov, T. Keith, R. Kobayashi, J. Normand, K. Raghavachari, A. Rendell, J. C. Burant, S. S. Iyengar, J. Tomasi, M. Cossi, J. M. Millam, M. Klene, C. Adamo, R. Cammi, J. W. Ochterski, R. L. Martin, K. Morokuma, O. Farkas, J. B. Foresman, and D. J. Fox, Gaussian, Inc., Wallingford CT, 2016.
11. A. C. Neto, F. E. Jorge, *Chem. Phys. Lett.*, 2013, **582**, 158-162.
  12. R. F. W. Bader, Atoms in Molecules - A Quantum Theory, Oxford University Press, Oxford, 1990.
  13. H. Jacobsen, *Canad. J. Chem.*, 2008, **86**, 695-702.
  14. T. Lu, F. Chen, *J. Comput. Chem.*, 2011, **33**, 580-592.
  15. E. V. Bartashevich and V. G. Tsirelson, *Russ. Chem. Rev.*, 2014, **83**, 1181-1203.